Photoemission from graphite: Intrinsic and self-energy effects

V N Strocov, Anne Charrier, J-M Themlin, M. Rohlfing, R. Claessen, N. Barrett, J. Avila, J. Sanchez, M.-C. Asensio

Photoemission from graphite: Intrinsic and self-energy effects

V. N. Strocov,* A. Charrier, and J.-M. Themlin
Groupe de Physique des Etats Condensés, UMR CNRS 6631, Université de la Méditerraneé, 13288 Marseille Cedex 9, France

M. Rohlfing
Institut für Theoretische Physik II, Universität Münster, D-48149 Münster, Germany

R. Claessen
Experimentalphysik II, Universität Augsburg, D-86135 Augsburg, Germany

N. Barrett
SPCSI-DRECAM-DSM, CEA Saclay, 91191 Gif-sur-Yvette Cedex, France

J. Avila, J. Sanchez, and M.-C. Asensio
Laboratoire pour l'utilization du Rayonnement Electromagnetique, Bâtiment 209D, Université Paris-Sud, Boîte Postale 34, 91898 Orsay Cedex, France

(Received 5 December 2000; revised manuscript received 23 March 2001; published 25 July 2001)

We report a photoemission study on high-quality single-crystal graphite epitaxially grown on SiC. The results are interpreted using independent information on the final states obtained by very-low-energy electron diffraction. Significant intrinsic photoemission and surface effects are identified, which distort the photoemission response and narrow the observed dispersion range of the π state. We assess its true dispersion range using a model photoemission calculation. A significant dependence of the excited-state self-energy effects on the wave-function character is found. The experimental results are compared with a *GW* calculation.

DOI: 10.1103/PhysRevB.64.075105 PACS number(s): 71.20.Tx, 79.60.−i, 71.20.−b, 71.10.−w

I. INTRODUCTION

The electronic structure of graphite, a prototype quasi-two-dimensional (quasi-2D) material, is important for understanding more complicated systems in this family, for example transition-metal dichalcogenides and HTSCs. Despite extensive studies, mainly using angle-resolved photoemission (PE) spectroscopy,[1,2] it remains far from being completely understood. In particular, knowledge about the 3D effects connected with remnant interlayer interaction is especially poor: a considerable disagreement remains between the experimental and calculated dispersion of the π state perpendicular to the layers.

Several problems complicate the interpretation of the PE spectra of graphite. That of the structural imperfection of available graphite single crystals is solved in this study using an epitaxial growth technique of sample preparation.[3,4,6] The intense secondary-electron (SE) structure in the PE spectra is reduced using the constant-final-state (CFS) mode of data acquisition. The prominent final-state effects, which are crucial for proper evaluation of the layer-perpendicular dispersions, are taken into account based on the recent information on the unoccupied states obtained by very-low-energy electron diffraction (VLEED).[7]

These approaches enabled us to reveal new intriguing properties of the electronic structure of graphite. In particular, we have found that the controversy regarding the π-band dispersion is mainly due to strong distortion of its PE response by intrinsic lifetime and surface effects. Deconvoluting of the intrinsic effects has allowed for a reliable comparison of the experimental results with density-functional theory (DFT) and quasiparticle band calculations. This has revealed strong excited-state self-energy effects whose band dependence correlates with the spatial localization of the one-electron wave functions.

II. EXPERIMENT

A. Sample preparation

The graphite sample was prepared by thermal epitaxial growth on the Si-terminated surface of 6H-SiC(0001). The substrate was cut from a commercial 0.3-mm-thick nitrogen-doped 6H-SiC wafer (CREE Research). It was fixed on a hollow Mo sample holder with an electron bombardment heating system on the underside. After introduction into the ultrahigh-vacuum chamber, the sample was heated to 850°C under a Si flux from a resistively heated Si wafer. This cleaning procedure, which removes the native surface oxide, leads to a Si-rich 3×3 reconstruction as observed by low-energy electron diffraction (LEED). The sample was then annealed for several minutes at temperatures above 1100°C without the Si flux. At this temperature, SiC dissociates and Si sublimates, leaving C-rich surface layers that tend to form a graphite structure.[3,4] These cycles were repeated several times increasing the annealing temperature up to 1400°C. The procedure gives a layer-by-layer growth of an epitaxial graphite film. Its crystallographic quality was ascertained by a sharp 1×1 LEED pattern without any visible rings, which would indicate an azimuthal disorder. The graphite film thickness was such that the SiC substrate could not be detected by LEED.

The resulting epitaxial film, as was demonstrated in our previous studies, is indistinguishable from a bulk graphite

crystal. First, this was confirmed by grazing-incidence x-ray diffraction (GIXD) experiments[5] in which the in-plane diffraction profiles gave the lateral lattice constant $a=2.451 \pm 0.01$ Å. It is in excellent agreement with the value $a=2.4589$ Å documented for single-crystal graphite. The epitaxial film is thus fully relaxed (no strain or reconstruction). Furthermore, the out-of-plane diffraction profiles confirmed the characteristic *ABAB* stacking. Interestingly, the lateral lattice constant remained essentially unchanged from the very first graphene plane. This demonstrates a very weak interaction of graphite with the SiC substrate, in contrast to metal substrates (e.g., Ni). Clearly, the epitaxy of graphite on SiC adopts the van der Waals mechanism, i.e., the substrate only orients the epitaxial layer without affecting the lattice parameters. Second, the whole body of the inverse PE,[6] VLEED, and PE data measured on the epitaxial film was compared with the available data measured on the single crystals. The comparison showed no notable differences in the electronic structure regardless of the orientation of the orbitals relative to the layers. This again implies the same lattice constants and a very weak interaction with the substrate. Furthermore, a high surface quality of the epitaxial film was confirmed by both GIXD and scanning tunneling microscopy (STM). They revealed the formation of flat terraces with the same orientation and an average width greater than 200 Å.

Epitaxial graphite samples have several advantages over natural or Kish single-crystal graphite. First, flexibility of the natural graphite crystals and inhomogeneity of their surface make it difficult to maintain uniform angular orientation of the sample surface. Second, the natural and Kish graphite crystals typically contain a few azimuthally misoriented crystallites. As the probing area often covers several crystallites, the angle-dependent measurements may become less reliable. In contrast, epitaxial graphite films grown on top of an electronic-grade SiC wafer polished to an optical finish have a very flat surface and truly single-crystal character.

B. Experimental results

The photoemission experiment on epitaxial graphite was performed at LURE, beamline SA73 (preliminary studies of the electronic-structure evolution during the graphite film growth were carried out on the Spanish beamline, SU8). The spectra were taken at normal emission, which corresponds to the layer-perpendicular ΓA direction of the bulk Brillouin zone (BZ). Linearly polarized monochromatic light from the plane grating monochromator was used with a polar incident angle of 45° and the electric vector lying in the plane of incidence containing the surface normal, giving thus equal amplitudes of the electric vector parallel and perpendicular to the surface. To cover a wide range of photon energies $h\nu$, we used two different gratings.

The experimental spectra taken in the energy-distribution-curve (EDC) mode (smoothed by Gaussian with a 50-meV half-width to reduced the noise) are shown in Fig. 1. Our results compare well with previous data obtained on natural single-crystal graphite,[1] but the spectra are ''cleaner'' in the sense of a better spectral contrast due to a better quality of epitaxial graphite. Also the SE intensity is lower due to relatively weak higher-order light.

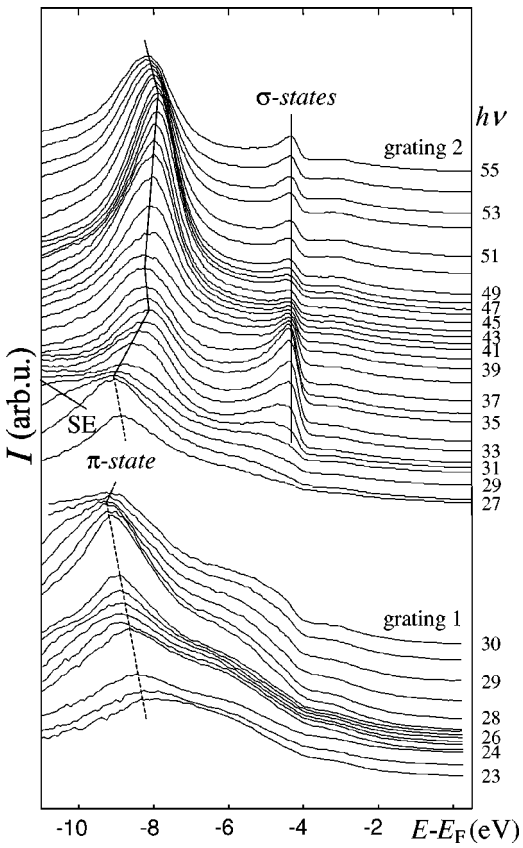

FIG. 1. Experimental normal-emission EDC spectra. Identification of the spectral peaks is shown. A reverse dispersion of the π-state peak in the low-energy final-state band gap (see the text below) is indicated by the dashed line.

In the low-energy region, the SE structures remain nevertheless rather intense, which can impair proper evaluation of the valence-band energies. To suppress their influence, in this region we have measured a series of spectra in the CFS mode by varying $h\nu$ with constant final-state energy E^f. In these spectra, the SE structures, which are characterized by $E^f=\text{const}$, form only a constant background and thus do not interfere with the peaks from the valence band. These spectra after the noise reduction are shown in Fig. 2. They were normalized to the photon flux using the current from a gold mesh installed after the exit slits of the monochromator.

The experimental spectra were insensitive to details of the sample preparation procedure. Only a shoulderlike structure near -5.6 eV, developing at low $h\nu$, showed some variations and reduced in amplitude upon improvement of the graphite film quality. Lying outside any band dispersion ranges or the regions of high density of states, this structure might not be intrinsic for graphite but due to a remnant signal from the SiC substrate or from Si atoms embedded in the film.

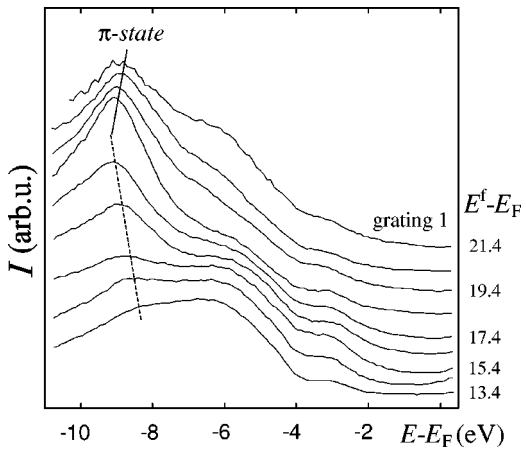

FIG. 2. Experimental normal-emission CFS spectra. The spectral peaks are identified as in Fig. 1.

III. DISCUSSION

A. π state

Analysis of the $k_\perp$ dispersions in the valence band requires, first of all, knowledge of the PE final bands. The corresponding $E(k_\perp)$ is described by complex $k_\perp$, whose imaginary part $\mathrm{Im}\,k_\perp$ accounts for the Bloch wave damping due to finite electron lifetime and coherent scattering off the crystal potential in the band gaps.

Recently, we have performed an independent study of the final bands of graphite using VLEED.[7] These bands demonstrated dramatic deviations from a free-electron-like dispersion due to strong perpendicular corrugation of the crystal potential resulting from the quasi-2D layered nature of graphite. The band gaps in the Γ point were found to extend from 10.8 to 18.6 eV and from $\sim$36.3 to 42.7 eV. In addition, we estimated the energy dependence of the electron absorption potential V_i, giving the final-state lifetime. These data, as demonstrated on certain transition-metal dichalcogenides,[8] allow us to obtain the final-state $k_\perp$ dispersions using a fitting procedure. In the present study, focusing on determination of the π-state dispersion range along the ΓA line, we will proceed with a simplified model for the final bands.

The final bands were modeled using the empirical pseudopotential method. The basis included only plane waves with the vectors $\mathbf{k}+\mathbf{G}$ perpendicular to the surface, which is sufficient for the main bands coupling to vacuum in the region of interest near the Γ point.[9] $E(k_\perp)$ was calculated by reducing the secular equation for complex $k_\perp$ to an eigenvalue problem.[10] The empirical parameters—the effective mass m^* and two relevant Fourier components—were determined by setting $V_i=0$ and fitting $E(k_\perp)$ to the two experimental band gaps in the Γ point. The calculated $E(k_\perp)$ is shown in Fig. 3. The dispersions are smoothed due to V_i. The photoelectron escape depth, determined by $\mathrm{Im}\,k_\perp$ as $\lambda=(\mathrm{Im}/k_\perp)^{-1}$, due to wide final-state band gaps dramatically deviates from the usual dependence of a monotonous increase upon decreasing $h\nu$. Note that by using the VLEED data, the obtained $E(k_\perp)$ incorporates the true non-free-electron and self-energy effects.

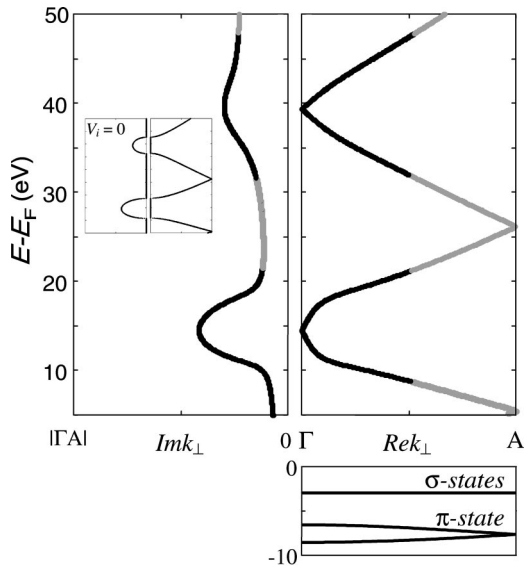

FIG. 3. $E(k_\perp)$ of the main PE final bands in the region of the band gaps in the Γ point (black lines) modeled using the VLEED data. Note the smoothing of the $k_\perp$ dispersion due to V_i and dramatic increase of $\mathrm{Im}\,k_\perp$ in the band gaps resulting in decrease of the photoelectron escape depth $\lambda=(2\,\mathrm{Im}\,k_\perp)^{-1}$. For clarity, the inset shows $E(k_\perp)$ for $V_i=0$. The lower panel shows the DFT-LDA calculated valence bands from Ref. 7 (in the photoemission process, **k** remains real, contrary to the final bands, because the initial-state wave function is almost undamped due to a very large absorption length of the light).

The experimental dispersion of the π-state peak in the PE spectra, intriguingly, deviates from that expected from the final-state $k_\perp$ dispersion. Indeed, the bottom of the π band in the Γ point (Fig. 3) is reached when the final bands pass this point in the lower-energy band gap at $E^f=14.5$ eV (taking into account the double-zone dipole selection rules[11]). One would expect that this energy delivers the dispersion minimum of the PE peak. However, in the experiment, the minimum is $\sim$4 eV higher in E^f, closer to the upper edge of the final-state band gap, with a *reverse dispersion* towards the middle of the gap. This effect does not occur for the upper edge of the π band, coupled to the higher-energy pass of the Γ point: $E^f=39.4$ eV predicted by the final state $E(k_\perp)$ agrees well with $E^f=40\pm0.5$ eV corresponding to the maximum of the PE peak dispersion.

The observed peculiarity of the PE response of the π state reveals that the analysis of the $k_\perp$ dispersions requires, besides knowing the final-state dispersions, accounting for *intrinsic effects* involved in the PE process that cause shifting of PE spectral peaks from the true quasiparticle bands, i.e., the dispersions of the peaks of the valence-band spectral function $A(\omega,\mathbf{k})$. These effects are essentially due to the final-state $k_\perp$ broadening $\mathrm{Im}\,k_\perp$ and the initial-state energy broadening $V_i^h=h/\tau$, where τ is the hole lifetime; their combination determines the profile of the PE peak, see, e.g., Refs. 12 and 13. Recently, it was noticed that if the initial-state $k_\perp$ dispersion is nonlinear, then the broadenings form an asymmetric PE peak with the maximum shifted from the energy, dictated by the direct transition, toward a larger inte-

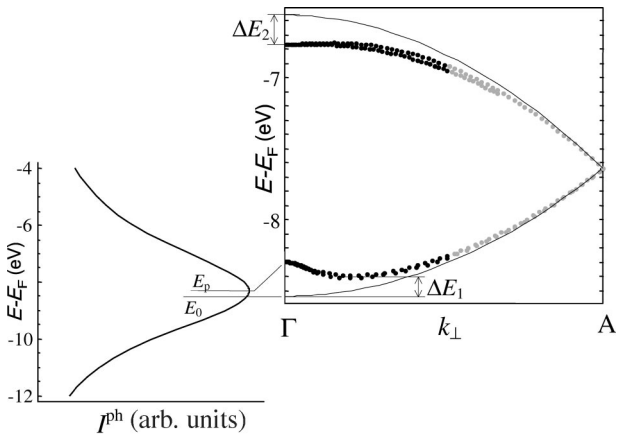

FIG. 4. Modeled PE response of the π state as the maxima of the PE peaks (dots, which line up in branches according to different final bands) on top of the true band dispersion. The deviations, particularly notable in the reverse dispersion near the band bottom, are the intrinsic shifts. The shown peak profile illustrates this effect for the band bottom; the peak maximum at E_p is shifted from E_0 dictated by the direct transition. The corrections applied to the experimental peak dispersion range are indicated.

gral number of states within the broadening profile.[14,15] Below, we will show that this intrinsic effect severely distorts the PE response of the π state.

We modeled the intrinsic effects using the VLEED-derived final bands and assuming the unperturbed bulk π band. The PE peak profiles were calculated by analytic integration[15] of the expression[12,13]

$$I(E^f) \propto \int_{-\infty}^{+\infty} \frac{1}{(k_\perp' - \mathrm{Re}\, k_\perp)^2 + (\mathrm{Im}\, k_\perp)^2} \times \frac{1}{[E^f - h\nu - E^i(k_\perp')]^2 + (V_i^h)^2} dk_\perp',$$

where the first term is the final-state Lorentzian $k_\perp$ distribution centered on the final-state $\mathrm{Re}\, k_\perp$, and the second is the initial-state energy distribution centered on the band dispersion $E^i(k_\perp)$. The matrix element and surface transmission factors were assumed to be constant. $E^i(k_\perp)$ was approximated by a quadratic dispersion fitted to the DFT calculations.[7] The V_i^h value of $\sim$1.9 eV, varying insignificantly within the band, was obtained from the experimental PE peak width using the known final state $\mathrm{Im}\, k_\perp$.

The results of modeling are shown in Fig. 4. In particular, near the band edges, as shown for the bottom of the π band, the peaks become asymmetric and shift from the position, dictated by the direct transition, into the band interior (in-band shifting) due to the absence of states beyond the band limits. This effect results in a deviation of the peak dispersion from the true $E(k_\perp)$, which is significant compared to the $k_\perp$ dispersion range (similar effects treated in the framework of one-step PE calculations are discussed in Ref. 16). We stress that this deviation is an intrinsic PE effect that has nothing to do with a deviation of the quasiparticle band from the ground-state picture (see below); it reflects how the quasiparticle band is measured in the PE experiment, and depends on the parameters of the selected final state.

The results give a good qualitative description of the experimental results. The reverse dispersion near the bottom of the π band occurs because the increase of $\mathrm{Im}\, k_\perp$ in the corresponding final-state band gap (Fig. 3) is exceptionally large due to a very large gap width and relatively small V_i. This results in an exceptionally large increase of the $k_\perp$ broadening and, therefore, in-band shifting, which overcomes the trend dictated by the final state $E(\mathrm{Re}\, k_\perp)$.[17] For the upper edge of the π band, coupled to the higher-energy final-state band gap, a similar effect is negligible because, due to the larger V_i and smaller gap width, the relative increase of $\mathrm{Im}\, k_\perp$ is much smaller. Note that if the final bands were described within the usual model of free-electron-like bands, the implied empirical adjustments would mimic the reverse dispersion and this intrinsic photoemission effect would be hidden.

The experimental reverse dispersion range is still $\sim$0.2 eV larger compared to the model calculation. Though small, this discrepancy may indicate two effects. First, it may have a contribution due to surface effects not included in the model calculation. As in the middle of the final-state band gap the valence-band wave function is probed at reduced λ compared to that near the gap edges ($\lambda \sim 0.8$ Å and 1.7 Å correspondingly, as determined from $\mathrm{Im}\, k_\perp$ in Fig. 3). The potential near the surface differs intrinsically from the ideally terminated bulk one due to overlap with the surface barrier and, probably, a minor relaxation of the interlayer distance. This causes a surface modification of the band structure in that the wave function differs from the ideally terminated bulk one, which may result in a shift of the PE peak. The same effect may occur near the upper edge of the π band ($\lambda \sim 1.2$ Å). Second, the phototransition matrix element may sharply decrease near the π band bottom, a rather common phenomenon for the sp bands, which, in combination with strong broadening of the PE peak, will result in its shift to higher energies.[8] The small value of the observed discrepancy suggests, however, that neither effect is pronounced.

To achieve the true π-band dispersion range, we first deconvoluted the intrinsic effects. The corresponding corrections were found near the band extrema from the above model calculations as shown in Fig. 4 (for the band bottom, we used the peak dispersion minimum away from the Γ point, where λ increases and the surface effects are reduced). With the experimental PE peak dispersing from -9.1 eV (determined from the CFS spectra) to -7.9 eV (EDC), we obtained the π-band dispersion range from -9.3 eV to -7.7 eV with the integral accuracy about ± 0.1 eV. Deconvoluting of the matrix element and surface effects is presumably also important, but their modeling requires slab band structure and one-step PE calculations, which are computationally difficult and has not been done in this work.

B. Excited-state self-energy effects

The experimental band energies were compared with the theoretical results, calculated in the DFT–local-density-approximation (LDA) framework using the first-principles

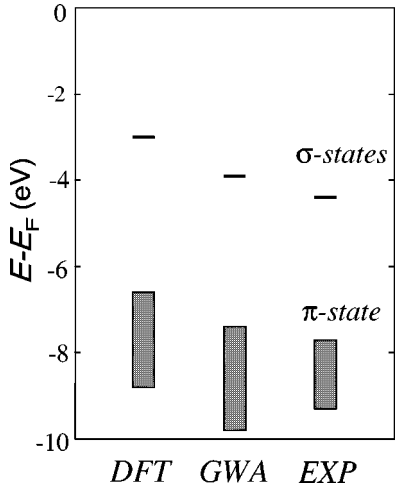

FIG. 5. Comparison of the experimental π- and σ-state energies with the DFT-LDA and quasiparticle GW calculations.

pseudopotential method (Fig. 5). The deviations are significant, on the whole $\sim$1 eV. In our case, the error introduced by the LDA is presumably insignificant (for the valence band, the LDA and generalized gradient approximation give almost identical results[7]). The deviations occur, therefore, because the dynamic electron exchange-correlation potential, expressed by the self-energy $\mathbf{\Sigma}$, differs from the static DFT one V_{xc}. The self-energy corrections to the band energies are determined by the expectation values $\Delta\Sigma = \langle \phi | \mathrm{Re}\,\mathbf{\Sigma} - V_{\mathrm{xc}} | \phi \rangle$. The observed $\Delta\Sigma$ show a band dependence: the σ states, despite being closer to E_F, are more strongly shifted compared to the π state.

The results of a first-principles quasiparticle calculation are also shown in Fig. 5. The self-energy operator was evaluated here within the GW approximation based on the DFT-LDA pseudopotential scheme.[18,19] The calculation reproduces well the direction and average magnitude of the $\Delta\Sigma$ shifts to within a few tenths of an eV.

The band dependence of $\Delta\Sigma$ may be related to the spatial localization of the one-electron wave functions determined by their overlap with the varying valence electron density $n(\mathbf{r})$ (the core electrons make a negligible contribution to the dynamic self-energy effects in the valence band due to large energy separations and thus weak virtual scattering from them).[15,20] This effect can be expressed through an effective wave-function-weighted density $\langle n \rangle = \int n(\mathbf{r}) |\phi(\mathbf{r})|^2 d\mathbf{r}$. The calculation in Fig. 6 shows that the π states are weighted mainly in the interlayer region. They experience thus a small effective $\langle n \rangle = 0.105\ (\mathrm{a.u.})^{-3}$. The σ states are weighted, on the contrary, within the layers with large electron density and experience a large $\langle n \rangle = 0.208(\mathrm{a.u.})^{-3}$. Concomitantly, the σ states have a much stronger expectation value $\langle \sigma | \mathrm{Re}\,\mathbf{\Sigma} | \sigma \rangle$ of the self-energy, in our GW calculation -17.3 eV, than the π state value $\langle \pi | \mathrm{Re}\,\mathbf{\Sigma} | \pi \rangle = -13.1$ eV. This effect, however, is already found within the DFT-LDA, which yields almost the same difference between $\langle \sigma | V_{\mathrm{xc}} | \sigma \rangle$ and $\langle \pi | V_{\mathrm{xc}} | \pi \rangle$. The GW calculated $\Delta\Sigma$ are therefore basically equal for both states. Nevertheless, for many systems such as Cu the dynamic exchange-correlation has a stronger dependence on the electron density than the static one, and a stronger localization of a state in a high-density region with a larger value of $\langle n \rangle$ leads to a stronger $\Delta\Sigma$.[15,20] The observed band dependence of $\Delta\Sigma$ in Fig. 5 seems to indicate that this behavior is also present in graphite. It is an open question as to why this effect is not found in the present GW results. It should be noted that an analysis of the specific physical origins of the $\Delta\Sigma$ shifts is highly sensitive to the numerical accuracy of the GW and DFT calculations, as the difference between the dynamic and static exchange-correlation is normally less than 10% of the total value.

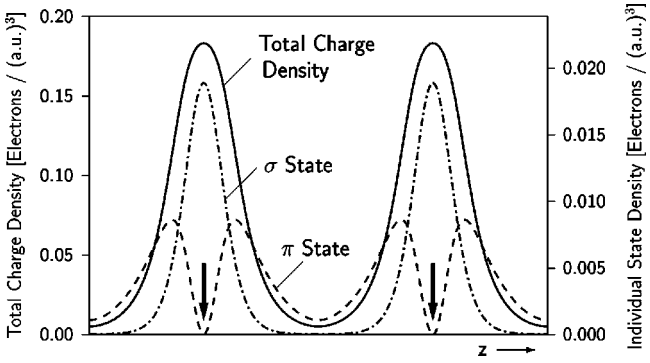

FIG. 6. Total valence charge density $n(\mathbf{r})$ and individual charge density $|\phi(\mathbf{r})|^2$ of the σ state and of the π state (averaged along the graphene layers) depending on the layer-perpendicular z coordinate perpendicular to the layers. The vertical arrows indicate the position of the graphene layers.

IV. CONCLUSION

Refined PE measurements on graphite have been performed using an epitaxially grown high-quality sample. The valence band along the layer-perpendicular ΓA line of theBZ was studied in detail. Interpreted using VLEED experimental data on the final bands, the PE data have revealed new peculiarities of the electronic structure of this prototype layered material. (i) PE response of the π band is severely distorted by intrinsic broadening effects, which narrow the observed band dispersion and can even reverse it. Similar effects can occur in other layered materials whose final bands are highly structured due to their quasi-2D nature. The experimental data deconvoluted from the intrinsic effects place the π band along the ΓA line from -9.3 to -7.7 eV, but these figures are still to be improved against the surface and matrix element effects. (ii) The experimental valence band experiences significant excited-state self-energy effects whose band dependence is connected with the spatial localization of the one-electron wave functions.

*Present address: Experimentalphysik II, Universität Augsburg, D-86135 Augsburg, Germany, and the Institute for High-Performance Computations and Databases, P.O. Box 71, 194291 St. Petersburg, Russia.

[1] A.R. Law, M.T. Johnson, and H.P. Hughes, Phys. Rev. B **34**, 4289 (1986).

[2] C. Heske, R. Treusch, F.J. Himpsel, S. Kakar, L.J. Terminello, H.J. Weyer, and E.L. Shirley, Phys. Rev. B **59**, 4680 (1999).

[3] A.J. Van Bommel, J.E. Crombeen, and A. Van Tooren, Surf. Sci. **48**, 463 (1975).
[4] L. Muehlhoff, W.J. Choyke, M.J. Bozack, and J.T. Yates, J. Appl. Phys. **60**, 2842 (1986).
[5] A. Charrier, A. Coati, F. Thibaudau, J.-M. Debever, M. Sauvage-Simkin, Y. Garreau, R. Pinchaux, and J.-M. Themlin (unpublished).
[6] I. Forbeaux, J.-M. Themlin, and J.-M. Debever, Phys. Rev. B **58**, 16 396 (1998).
[7] V.N. Strocov, J.-M. Themlin, J.-M. Debever, H.I. Starnberg, P. Blaha, M. Rohlfing, and R. Claessen, Phys. Rev. B **61**, 4994 (2000).
[8] V.N. Strocov, H. Starnberg, P.O. Nilsson, H.E. Brauer, and L.J. Holleboom, Phys. Rev. Lett. **79**, 467 (1997); J. Phys.: Condens. Matter **10**, 5749 (1998).
[9] Our modeling misses therefore the band gaps due to hybridizatin with other plane waves. Most notable of such band gaps is placed near 30 eV (see Ref. 7). In the PE spectra, the corresponding distortion of the final-state dispersion is reflected by distorted dispersion of the π state peak in the $h\nu$ range from 32 to 38 eV, see Fig. 1.
[10] J.B. Pendry, J. Phys. C **2**, 2273 (1969).
[11] D. Pescia, A.R. Law, M.T. Johnson, and H.P. Hughes, Solid State Commun. **56**, 809 (1985).
[12] *Angle-Resolved Photoemission*, edited by S.D. Kevan (Elsevier, Amsterdam, 1992).
[13] R. Matzdorf, Appl. Phys. A: Mater. Sci. Process. **63**, 549 (1996).
[14] V.N. Strocov, in *Electron Spectroscopies Applied to Low-dimensional Materials* (Kluwer, The Netherlands, 2000).
[15] V. N. Strocov *et al.*, Phys. Rev. B **63**, 205108 (2001).
[16] E. Pehlke and W. Schattke, Solid State Commun. **69**, 419 (1989); T. Strasser, F. Starrost, C. Solterbeck, and W. Schattke, Phys. Rev. B **56**, 13 326 (1997).
[17] The reverse dispersion may in principle limit the accuracy of the three-dimensional band mapping using the band-gap emission [V.N. Strocov *et al.*, Phys. Rev. Lett. **81**, 4943 (1998) and Ref. 15], but it appears only in exceptionally wide final-state band gaps.
[18] M.S. Hybertsen and S.G. Louie, Phys. Rev. Lett. **55**, 1418 (1985); Phys. Rev. B **34**, 5390 (1986).
[19] M. Rohlfing, P. Krüger, and J. Pollmann, Phys. Rev. B **52**, 1905 (1995).
[20] P.O. Nilsson and C.G. Larsson, Phys. Rev. B **27**, 6143 (1983).